IEEE Access
Multidisciplinary | Rapid Review | Open Access Journal

Received May 29, 2019, accepted June 10, 2019, date of publication June 14, 2019, date of current version July 1, 2019.

Digital Object Identifier 10.1109/ACCESS.2019.2923185

Artificial Intelligence to Design a Mask Insensible to the Distance From the Camera to the Scene Objects

SERGIO LEDESMA[1,2], MARIO-ALBERTO IBARRA-MANZANO[1], (Member, IEEE), EDUARDO CABAL-YEPEZ[1], (Member, IEEE), DORA-LUZ ALMANZA-OJEDA[1], AND PASCAL FALLAVOLLITA[2]

[1]School of Engineering, University of Guanajuato, Salamanca, GTO 36885, Mexico
[2]Interdisciplinary School of Health Sciences, Faculty of Health Sciences, University of Ottawa, Ottawa, ON K1N 7K4, Canada

Corresponding author: Sergio Ledesma (selo@ugto.mx)

ABSTRACT The sharpness of an image depends on the spatial frequency response of the photographic imaging system and the sensor characteristics. In conventional digital cameras, only those objects within a distance range are in focus, while other objects are captured with different amounts of blurring depending on their distance to the focal plane. This can be desired for some applications; however, this can also be undesired because some objects in the scene may be blurred and impossible to recover. In the field of augmented reality, simulating this natural effect of showing sharp objects in combination with blurred objects increases the visual realism of augmented video. In order to simulate this effect, it is very important to capture all objects in the scene with high quality so that it could be possible to dynamically blur different objects in the scene at runtime. In this paper, we present an algorithm to find a set of possible complex-amplitude transmittance masks capable of considerably reducing the impact of focus errors in the scene objects. Computer simulations are used to compare the masks found in this paper with a classic mask in the state of the art. The main contribution of this paper is the use of Chebyshev polynomials to model an optical mask, and then, use artificial intelligence to establish some properties of this mask, such as the depth of field, the resolution, and the amount of gathered light.

INDEX TERMS Artificial intelligence, blurring in an image, high-resolution imaging, image processing, multi-focus image, simulated annealing.

I. INTRODUCTION

Because of the limited depth of field (DOF) of conventional digital cameras, only those objects within a certain distance range are in focus [1], [2]. In fact, those objects outside the depth of field are captured with different amounts of blurring depending on their distance to the focal plane. This limited depth of field can be desired if, for instance, information on the alignment of a three-dimensional specimen is needed [3]. In some specific cases, low depth of field is desired, such as in portrait photography or movies to attract the viewer's attention to a particular region or scene [4]. However, for some other applications, an extended depth of field is required because some objects in the scene may be blurred. In the field of augmented reality, the depth of field "effect" increases the visual realism of augmented video. In fact, if the DOF is ignored, very close or distant virtual objects which are out of the camera's focus still appear sharp and focused in the image, and consequently, they look unnatural and can degrade the visual coherence of the video [5]–[8]. In order to provide a natural effect in augmented reality, it is usually necessary to capture the depth perception using a depth sensor such as in: Microsoft Hololens, Meta 2, or DAQRI Smart Glasses, [9].

The frequency response of an optical system determines the quality and the amount of detail of the captured image. However, the frequency response of this type of systems is affected by the distance between the lenses and the objects in the scene. One of the main challenges when capturing an image is to have an optical system with a frequency

The associate editor coordinating the review of this manuscript and approving it for publication was Zijian Zhang.

response that is not significantly affected by this distance. One common method to reduce these changes in the frequency response is by reducing the size of the aperture. Unfortunately, a small aperture introduces a high energy-attenuation, and consequently, cannot be used unless the objects in the scene are exposed to a powerful source of light. In this sense, the main challenge is to design an optical mask that introduces little energy-attenuation and has a similar frequency response for all objects in the scene.

In this work, a method to find an optical mask that is not affected by the distance from the camera to the objects in the scene is proposed. The main contribution is a transmittance model for an optical mask using Chebyshev polynomials. Another contribution is the use of a hybrid method based on simulated annealing and Powell's method in multi-dimensions to find the coefficients of the Chebyshev polynomials, and consequently, design an optical mask with some desired properties. In other words, our method uses simulated annealing to explore the possible existence of one or more masks with these properties. An additional contribution is the design of an error function that incorporates three of the most important properties for extending the depth of field: the frequency response variability, the frequency bandwidth, and the energy-attenuation.

After the execution of the Artificial Intelligence algorithm, the obtained results show that there are four possible masks that can be used to increase the depth of field of an optical system, that is, these four masks are able to capture high-quality images with objects located at different distances from the camera. To test the effectiveness of our method, these four masks were compared with two classical masks in the state of the art.

Section II briefly describes key concepts for extending the depth of field of an optical system. This section ends by presenting some of the most important methods in the state of the art for extending the depth of field: the cubic phase mask, the Gaussian apodizing filter and the sub Gaussian window. Section III introduces Chebyshev polynomials and their properties. Section IV presents an optimization technique from the area of Artificial Intelligence called simulated annealing. Section V reviews Powell's method in multi-dimensions. Section VI introduces the method proposed in this work. Finally, Section VII presents the results obtained from the computer simulations.

II. THE DEPTH OF FIELD

The depth of field is the distance between the nearest object and the farthest one in a scene when both objects are captured by an imaging system with an acceptable sharp focus. The depth of field declines as magnification increases. This is very important in microscopy. For instance, when looking at tissues from plants or animals that are two or more cell layers deep [16]; at low magnification, it may be possible to get both cell layers in focus at the same time, but at high magnifications, when one cell layer is in focus, the other layer will be blurry. For movie production, the authors of [17] concluded that the three most effective features to distinguish professional video shots from amateur ones are the camera motion, the shot length, and the depth of field.

The Optical Transfer Function (OTF) of an optical system indicates how each spatial frequency is being processed by the system. The magnitude of the OTF is the Modulation Transfer Function (MTF), therefore

$$MTF(\mu, W) = |OTF(\mu, W)|\,, \tag{1}$$

where μ is the spatial frequency, and W represents the wavefront focus coefficient $W_{2,0}$ measured in wavelengths. In other words, W is the one-dimensional version of the Hopkins focus error coefficient. The Modulation Transfer Function indicates how much of the image contrast is preserved for each value of the spatial frequency μ. The impact of the focus error on the MTF restricts the longitudinal range, in the object space, for acquiring high-quality pictures. In the state of the art, the acceptable longitudinal range is denoted as the depth of field (DOF), [18].

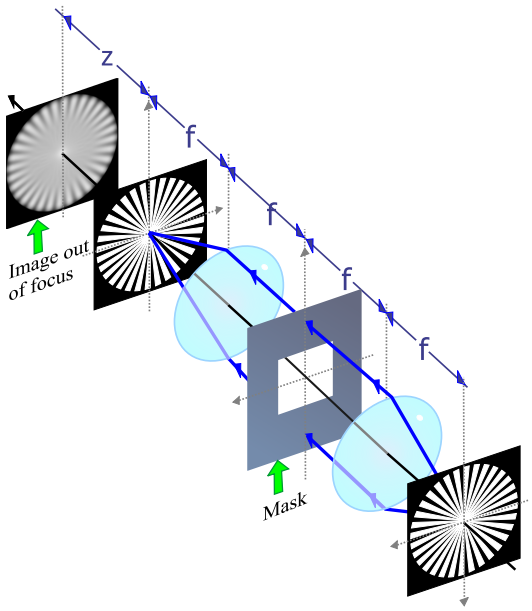

FIGURE 1. Optical system.

Figure 1 shows the schematic diagram of an optical system. For the sake of clarity, the following discussion is performed using one-dimension. However, it can be easily generalized to two-dimensions. The optical system in Figure 1 can be represented by a generalized pupil function whose complex amplitude transmittance is

$$P(\mu, W) = \Delta(\mu) \exp\left[i\,2\pi W \left(\frac{\mu}{\Omega}\right)^2\right] \tag{2}$$

where $\Delta(\mu)$ is the complex amplitude transmittance of a mask and Ω denotes the cut-off spatial frequency of the

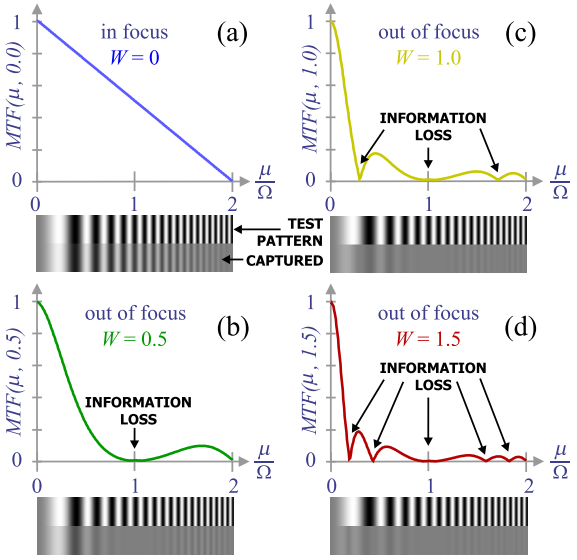

FIGURE 2. MTF for a rectangular mask, $\Delta(\mu) = \Pi(\frac{\mu}{2\Omega})$. (a) in focus W=0, (b) out of focus W=0.5, (c) out of focus W=1.0, (d) out of focus W=1.5.

pupil aperture. The normalized irradiance distribution of the impulse response as a function of the focus error is

$$h(x, W) = |p(x, W)|^2. \tag{3}$$

By applying the inverse Fourier Transform to Equation 3, we get

$$h(x, W) = \left| \int_{-\infty}^{\infty} P(\mu, W) \exp(i\, 2\pi x \mu) d\mu \right|^2. \tag{4}$$

Therefore, the MTF is

$$MTF(\mu, W) = |H(\mu, W)|\,. \tag{5}$$

Now, if we apply the Fourier Transform to Equation 5, we get

$$MTF(\mu, W) = \left| \int_{-\infty}^{\infty} h(x, W) \exp(-i\, 2\pi x \mu) dx \right|. \tag{6}$$

Finally, after substituting Equation 3 in Equation 6, we get

$$MTF(\mu, W) = \left| \int_{-\infty}^{\infty} |p(x, W)|^2 \exp(-i\, 2\pi x \mu) dx \right|. \tag{7}$$

Figure 2 shows the MTF when $\Delta(\mu) = \Pi(\frac{\mu}{2\Omega})$. Here, $\Pi(x)$ is the rectangular function defined as

$$\Pi(\frac{\mu}{2\Omega}) = rect(\frac{\mu}{2\Omega}) = \begin{cases} 0 & \text{if } |\mu| > \Omega \\ \frac{1}{2} & \text{if } |\mu| = \Omega \\ 1 & \text{if } |\mu| < \Omega \end{cases} \tag{8}$$

that is, the function is zero for any frequency bigger than Ω or any frequency lower than $-\Omega$. In order to compare the performance of an optic system (and a mask), a test pattern may be used, see Figure 2. The test pattern in Figure 2 contains several spatial frequencies. Starting on the left, the pattern begins with a very low frequency resulting in a big spacing between the vertical lines. As we move from left to right in the pattern, the spatial frequency gradually increases, and therefore, the distance between the lines decreases. This pattern is useful because it allows observing the performance of an optic system at several frequencies. In fact, by comparing the test pattern with the captured image of the pattern, it is possible to understand how the system will generally perform with most images. Figure 2.a shows the MTF when $W = 0$, that is, when the object being captured is in focus. In this case, the MTF decreases linearly when the frequency increases. The test pattern at the bottom of the graph in Figure 2.a indicates that despite the attenuation at high frequencies, image information is preserved for most frequencies. This is the ideal case, however, under normal circumstances, the objects in the scene are placed at different distances from the camera and different MTFs are used to process each object. In fact, if an object is big and the camera is close to the object, several MTFs will be used to process each part of the same object. This is very important when the depth of field is simulated in augmented reality. Figure 2.b shows the MTF when $W = 0.5$. In this case, the MTF exhibits a considerable attenuation in the middle of the pattern. Consequently, areas of the image with these spatial frequencies will be lost when the MTF is zero. When the MTF is small but not zero, the areas of the image affected by this attenuation will have very low contrast. In practice, an image usually has several frequency values in the same area, therefore, when parts of the image with medium or high-frequency values are attenuated, it will result in a detail loss in the image. Figures 2.c and 2.d show the MTF when $W = 1.0$ and $W = 1.5$ respectively. As it can be seen from Figure 2, the shape of the MTF under misfocus is significantly different from the shape of the MTF in focus, [19]. In fact, the shape of the MTF changes considerably for each value of W.

A. RELATED WORK

In the last few decades, there has been a great amount of research to increase the depth of field [10]. One common approach to extend the depth of field is by using an array of lenses in combination with computing-intensive algorithms that must be calibrated every time to reach in-focus images, as indicated in [11]. However, in this type of approaches, some information and resolution from the image are lost [12]. In [13], the performance benefit of a Light Field camera for extending the depth of field over other camera designs is shown, see also [14]. Other approaches include the use of an optical mask. These approaches will be discussed next.

1) CUBIC PHASE MASK

The cubic phase mask is one of the most common and widely used approach for increasing the depth of field [20]. For the cubic phase mask in [11] and [21], the complex amplitude transmittance of the pupil aperture is

$$\Delta(\mu) = \exp\left(i2\pi\rho(\frac{\mu}{\Omega})^3\right) \Pi\left(\frac{\mu}{2\Omega}\right) \tag{9}$$

where ρ is the maximum value of the optical path difference introduced by the mask, in units of λ. For this mask, the MTF

does not exhibit any zero values in the passband. However, the MTF presents some oscillations around the mean value line [22].

2) GAUSSIAN APODIZING FILTER

In order to reduce the oscillations introduced by the cubic phase mask in Equation 9, the authors of [22] proposed the use of a weak Gaussian filter in combination with the cubic phase mask, thus the complex transmittance of the mask is defined as

$$\Delta(\mu)=\exp\left(-2\pi\tau(\frac{\mu}{\Omega})^2\right)\exp\left(i2\pi\rho(\frac{\mu}{\Omega})^3\right)\Pi\left(\frac{\mu}{2\Omega}\right) \quad (10)$$

where τ is an attenuation factor to change the half-width of the apodizing filter.

3) FRACTIONAL WAVEFRONT MASK COMBINED WITH A SUB GAUSSIAN WINDOW

The authors of [15] explored the use of fractional phase variations combined with a sub Gaussian amplitude transmittance as in Equation 11. Ojeda et al. concluded that their method substantially reduced the mean square error of the MTF vs. focus errors, as well as unwanted oscillations in the MTF around its tendency curve. There are some differences between the mask in Equation 10 and the mask in Equation 11. The main difference is the exponent of the amplitude component, in Equation 10 the exponent has a value of two, while in Equation 11 its value 1.75; this is why this mask is called sub-Gaussian.

$$\Delta(\mu)=\exp\left(-2\pi\tau|\frac{\mu}{\Omega}|^{1.75}\right)\cdot\exp\left(i2\pi\rho\, sgn(\mu)|\frac{\mu}{\Omega}|^{2.75}\right)\cdot\Pi\left(\frac{\mu}{2\Omega}\right) \quad (11)$$

III. CHEBYSHEV POLYNOMIALS

The Chebyshev polynomials are a sequence of orthogonal polynomials, which can be recursively defined. The Chebyshev polynomial of degree n is denoted by $T_n(x)$, and is defined as

$$T_n(x)=\cos(n\times\arccos(x)). \quad (12)$$

For function approximation, the Chebyshev polynomials of the first kind T_n, and the Chebyshev polynomials of the second kind U_n can be used [23]. Because both, the polynomials of the first kind and of the second kind provide similar performance for function approximation, in this work, only the polynomials of the first kind are considered for approximating a set of optical masks. The Chebyshev polynomials are plotted in Figure 3.a and they are defined as

$$\begin{aligned}T_0(x)&=1\\T_1(x)&=x\\T_2(x)&=2x^2-1\\T_3(x)&=4x^3-3x\\&\cdots\\T_{n+1}(x)&=2xT_n(x)-T_{n-1}(x)\quad n\geq 1.\end{aligned} \quad (13)$$

In polynomial approximation the roots of the Chebyshev polynomials of the first kind are called Chebyshev nodes

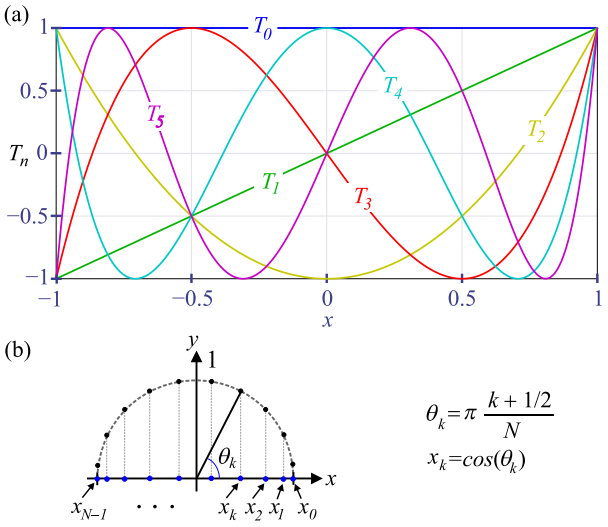

FIGURE 3. (a) Chebyshev polynomials of the first kind $T_n(x)$ (b) Chebyshev nodes.

because in these points (nodes) the polynomial approximation coincides exactly with the actual function value. Figure 3.b shows how the Chebyshev nodes, $x_0, x_1, \cdot, x_{N-1}$ are distributed. By inspecting the location of the nodes, it is possible to show that a Chebyshev expansion is similar to a Fourier cosine transformation with some changes of variables. In the suitable Sobolev space, the Chebyshev polynomials can be used to create a orthonormal basis. Therefore, these polynomials can be utilized to express a function $f(x)$ as a Chebyshev expansion when $-1\leq x\leq 1$ as

$$f(x)=\sum_{n=0}^{\infty}c_nT_n(x). \quad (14)$$

where c_n are some coefficients that must be determined. A function approximation using the Chebyshev polynomials is not necessarily more accurate than some other approximating polynomial of the same order, but rather the series expansion of Equation 14 can be truncated to a polynomial of lower degree in a very graceful way, one that does yield the most accurate approximation [23].

IV. SIMULATED ANNEALING

Simulated annealing is an optimization technique that can be used where exact methods do not exist or where deterministic methods are computationally too complex to implement [24]. One of the main advantages of simulated annealing is that it is able to avoid false local minima [23]. Simulated annealing is inspired in the process a substance goes through when it is heated until it reaches its fusion point to liquefy it, and then slowly cooled down in a controlled manner until it solidifies back [25].

To design and optimize an optical mask using simulated annealing, the structure of the substance represents a possible mask, and the temperature is used to determine how and when new masks are modified and accepted. In this case,

simulated annealing is mainly a three steps process: randomly modify the mask, evaluate the performance of the mask, and accept the mask if it is better than the best mask so far [26]. The metropolis algorithm is typically used to compute the probability to accept a solution (a new mask).

$$p_a = \begin{cases} \exp(-\frac{g\Delta E}{T}), & \Delta E > 0 \\ 1, & \Delta E \leq 0 \end{cases} \tag{15}$$

where p_a is the probability of acceptance, g is a constant, ΔE is the error difference between two solutions (two possible masks) and T is the temperature.

V. POWELL'S METHOD IN MULTI-DIMENSIONS

In most cases, the result obtained by the algorithm of simulated annealing can be improved by using an efficient multi-dimensional minimization algorithm. For this particular application, derivatives are not directly available, thus a method that requires only function evaluation may be used. Two common methods that do not require derivatives are the downhill simplex method and Powell's method in multi-dimensions [23]. For most applications, Powell's method is faster than the downhill simplex method [23]. In this case, the design of an optical mask can be seen as the process of finding the minimum (or maximum) of an objective function in a multi-dimensional space. While the algorithm of simulated annealing is not very efficient when compared with other minimization methods, it is not easily foul with false minima as other multi-dimensional minimization algorithms are. Thus, the optimization method in this paper is described as follows. First, simulated annealing is used to find a global minimum, and consequently, create a draft (or sketch) of the optical mask. Then, Powell's method is used to refine (or improve) the mask.

VI. PROPOSED METHOD

One easy method to increase the depth of field is by reducing the aperture of the pupil. However, small apertures (f/16, f/22 or f/32) considerably reduce the amount of light captured by the system, additionally, the image may be affected by diffraction. This paper proposes a method to explore the possible existence of a mask (or a set of masks) capable of extending the depth of field without varying the size of the pupil aperture but instead introducing a slight attenuation. Consequently, the value of Ω is assumed to be the same for all the masks in the simulations.

In this study, we propose the use of Chebyshev polynomials to model a mask for extending the depth of field. Additionally, we propose the use of one technique from the field of Artificial Intelligence called simulated annealing to estimate the values of the coefficients of the Chebyshev polynomials. Simulated annealing is used to perform a search for an optical mask with the best performance according to a defined error function. In this sense, the design of an optical mask can be seen as an optimization process. Thus simulated annealing is used to obtain an initial value for the coefficients of the Chebyshev polynomials. Then, the optimization process continues using Powell's method in multi-dimensions to further reduce the value of the error. The error function in this work incorporates some of the most important properties to attain an extended depth of field.

A. CHEBYSHEV MASKS

In order to find the existence of a possible mask to extend the depth of field, we propose to model the mask amplitude using Chebyshev polynomials as

$$\begin{aligned} \textit{Mask Amplitude} &= |\Delta(\mu)| \\ &= \Pi\left(\frac{\mu}{2\Omega}\right)\sum_{n=0}^{A} a_n T_n\left|\frac{\mu}{2\Omega}\right| \end{aligned} \tag{16}$$

where $\Pi(\mu/2\Omega)$ is defined as in Equation 8, T_n are the polynomials of the first kind in Equation 13, A is the number of terms used to approximate the amplitude of the mask, and a_n are some coefficients that need to be determined. Similarly, to model the phase of the mask, we propose

$$\begin{aligned} \textit{Mask Phase} &= \measuredangle[\Delta(\mu)] \\ &= \sum_{n=0}^{B} b_n T_n\left(\frac{\mu}{2\Omega}\right) \end{aligned} \tag{17}$$

where B is the number of terms used to approximate the phase of the mask, and b_n are some coefficients that need to be determined. By combining Equation 16 and Equation 17, we obtain an expression for the transmittance of the mask as

$$\begin{aligned} \Delta(\mu) = \Pi\left(\frac{\mu}{2\Omega}\right)&\left[\sum_{n=0}^{A} a_n T_n\left|\frac{\mu}{2\Omega}\right|\right] \\ &\times \exp\left[i\,2\pi\sum_{n=0}^{B} b_n T_n\left(\frac{\mu}{2\Omega}\right)\right] \end{aligned} \tag{18}$$

this last expression is one of the main contributions of this work because it provides an ample domain of functions to consider for the Artificial Intelligence algorithm. In fact, the only limits impost by this equation are the values of A and B that have to be finite value for simulations purposes. For the computer simulations of Section VII, the values of A and B were set to five. Bigger values than five were tested, but no further improvements were observed.

B. VARIATIONS IN THE MTF WHEN W CHANGES

A quick inspection in the graphs in Figure 2 reveals that the shape of the MTF changes when W changes. This is not desired because it would be difficult to try to restore the image by applying a single filter as different objects in the scene may require different types of compensation. Thus, one of the main objectives of this work is to find a mask with an MTF that does not change when W changes. In order to create an objective function to measure the changes in the MTF, suppose that there is a set $\{W_1, W_2, \cdots, W_M\}$ with M values for the wavefront focus coefficient. Assume also that there is another set $\{\mu_1, \mu_2, \cdots, \mu_N\}$ with N values for the spatial frequency. Figure 4 displays the MTF for all values of W and all values of μ in the sets. The green arrows in

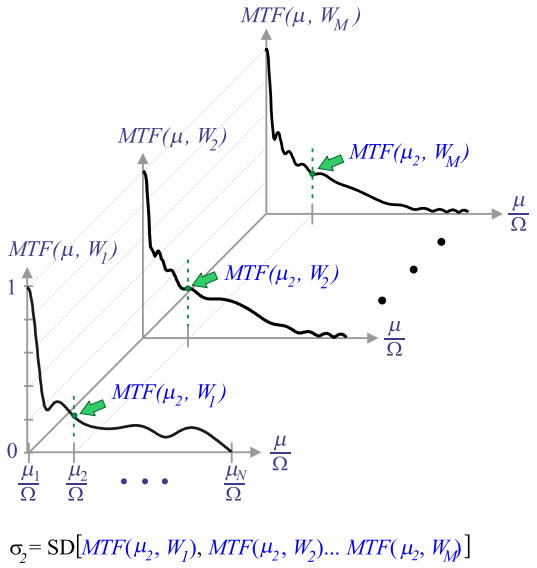

FIGURE 4. Computation of σ_2.

the figure display the M values for the MTF when the spatial frequency is equal to μ_2. Note that this value is only chosen for illustrative purposes. A quick method to measure the changes of the MTF is by computing the standard deviation for each spatial frequency as

$$\begin{aligned} \sigma_1 &= SD\left[MTF(\mu_1, W_1), \cdots, MTF(\mu_1, W_M)\right] \\ \sigma_2 &= SD\left[MTF(\mu_2, W_1), \cdots, MTF(\mu_2, W_M)\right] \\ &\cdots \\ \sigma_N &= SD\left[MTF(\mu_N, W_1), \cdots, MTF(\mu_N, W_M)\right] \end{aligned} \quad (19)$$

Figure 4 shows how to compute the value of σ_2. Other values for σ are computed similarly. Equation 19 indicates that there are N standard deviation values, one for each spatial frequency in the set. Each standard deviation, σ_1, σ_2, $\cdots$, σ_N, represents the changes in the MTF when W changes. Therefore, it is desired that $\sigma_1 \approx 0$, $\sigma_2 \approx 0$, $\cdots$, $\sigma_N \approx 0$, so that the MTF remains almost constant when W changes. As the algorithm of simulated annealing requires only a single value to measure the error of the solution, we need to combine the values of σ_1, σ_2, $\cdots$, σ_N into a single value. We consider the average and maximum value to combine the standard deviation values; the results of the computer simulations revealed that the maximum value is more effective for the optimization process than the average value. Therefore, the objective function that measures the variations in the MTF when W changes is computed as follows

$$Error_{variations} = \max(\sigma_1, \sigma_2, \cdots, \sigma_N). \quad (20)$$

Thus, we desire $Error_{variations}$ to be as small as possible so that the MTF does not get affected by W. There are some nice properties about Equation 20. First, it ensures that all standard deviation values of the MTF are less than (or equal to) the maximum value, and second, it is easily and efficiently computed.

C. BANDWIDTH ERROR

As the depth of field decreases to allow high resolution, the blur may dominate, deteriorating the capability of standard methods to accurately register the input image [27]. Under misfocus, the MTF of a conventional optical system goes to zero at some frequencies [19] resulting in information loss. In fact, avoiding zero values in the MTF is very important because in this way all the information in the image is preserved, since zero values in the MTF mean that the image information has been completely lost at the corresponding frequencies.

One problem of Equation 20 is that if the MTF exhibits small values for several frequencies, then the resulting value for $Error_{variations}$ will be small. In order to correct this problem, we need to introduce a new term to compensate and prevent the MTF from going to zero. Assume that there is a threshold value β to represent a desired minimum value for the MTF. Assume also that δ represents the highest frequency value that can be obtained while keeping the value of the MTF above the value of β as in Figure 5.

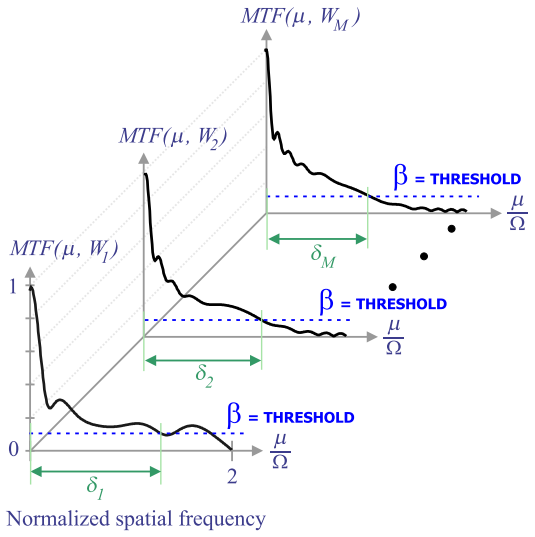

FIGURE 5. Computation of the bandwidth error.

Following this method, we can compute the values of δ_1, δ_2, $\cdots$, δ_M. One easy method to combine these values is as follows

$$Error_{bandwidth} = \frac{M}{\delta_1 + \delta_2 + \cdots \delta_M}. \quad (21)$$

When the values of δ_1, δ_2, $\cdots$, δ_M are big, the value of $Error_{bandwidth}$ is small. This indicates that a continuous big portion of the MTF is above the threshold β. Therefore, it is desired that $Error_{bandwidth}$ be as small as possible to promote that most values of the MTF are above the threshold β.

D. POWER ERROR

The last objective function is about the gathering of light power. As it is commonly known, a small aperture has an excellent depth of field, however, this is accomplished at the

expenses of a reduction in the light power captured by the optical system. In this paper, we would like to preserve the resolution associated with a full aperture, and an extended depth of field without sacrificing the amount of light. Therefore, trying to increase the amount of light power gathered by the system, we define

$$Error_{power} = 1 - \frac{1}{K}\int_0^2 |\Delta(\mu)|\, d\mu \tag{22}$$

where K is normalization constant so that

$$0 \leq Error_{power} \leq 1 \tag{23}$$

and $|\Delta(\mu)|$ is the magnitude of the transmittance of the mask. When $|\Delta(\mu)|$ is small, $Error_{power}$ will be close to one. On the other hand, when the magnitude of $|\Delta(\mu)|$ is big, $Error_{power}$ will be close to zero.

In order to produce one single objective function, it is necessary to combine Equation 20, Equation 21 and Equation 22. A straight forward method to combined these three equations is by using three priority parameters α_1, α_2, and α_3 as in Equation 24.

$$Error = \alpha_1(Error_{variations}) + \alpha_2(Error_{bandwidth}) + \alpha_3(Error_{power}) \tag{24}$$

where

$$\alpha_1 + \alpha_2 + \alpha_3 = 1. \tag{25}$$

Similarly, it can be concluded that other desired features in the MTF of the optical mask can be incorporate so that the mask can be implemented. This work only includes three of the most important properties to extend the depth of field. Future work may analyze other important characteristics for the actual implementation of this type of masks. One of the main important contributions of this work is the design of the three objective functions of Equations 20, 21 and 22.

VII. SIMULATION RESULTS

In order to test the method proposed in this paper, several computer simulations were performed to design different masks. The results in this section include four of the most relevant masks found. Other interesting masks can be found by using other setup parameters.

A. THE CUBIC PHASE MASK WITH A GAUSSIAN APODIZING FILTER

Figure 6 shows the MTF of a classic mask to extend the depth of field, see [11], [12], [21]. The complex transmittance of this mask is given in Equation 10. In this figure, the MTF was plotted for seven values of the wavefront focus coefficient W. As the MTF is very similar for all values of W, the graph looks like a single graph. At the top of Figure 6, the test pattern previously discussed is shown. Just under the test pattern, the figure displays the captured image using the cubic phase mask in combination with the gaussian apodizing filter. In order to make the simulation most realistic, the patter is

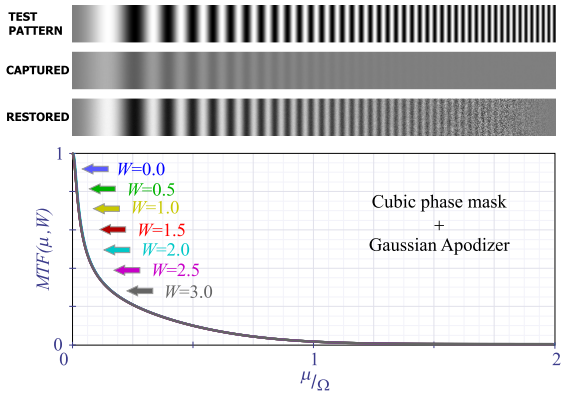

FIGURE 6. Cubic phase mask with the Gaussian apodizing filter.

contaminated with 0.5% of white noise. The main purpose of the noise is to simulate the noise present in the sensor. The value of 0.5% was chosen only to illustrative purposes, as real sensors have a very low noise level. Even though the captured image has been contaminated, the noise is not visible. The figure also shows the restored image that is obtained by using a filter to compensate for the impact of the MTF of the mask. As it can be seen, the restoration process is able to recover the high-frequency content of the image to the normal level as in an in-focus image, but at the same time, the noise is amplified resulting in a poor signal to noise ratio at high and very high frequencies.

B. THE FRACTIONAL WAVEFRONT MASK WITH SUB GAUSSIAN WINDOW

In this subsection, we evaluate the performance of the mask in Equation 11, see [15]. The MTF of this mask is very similar to the MTF in Figure 6. Nonetheless, the sub Gaussian exhibits less attenuation than the Cubic + Gaussian mask (in Figure 6) at mid frequencies. On the other hand, the Cubic + Gaussian mask has less attenuation than the sub Gaussian mask at low frequencies. Note that both masks exhibit a strong attenuation at high frequencies. These two masks are very common in the state of the art to extend the depth of field and are used here for comparative purposes. In the next subsection, we evaluate the performance of the masks proposed in this work.

C. CHEBYSHEV MASKS

This section analyzes the Chebyshev masks proposed in this paper. The values of A and B in Equation 18 were set to five. Bigger values were tested, but no further improvements were observed. The mask optimization process to find the values of a_n and b_n in Equation 18 was performed in two steps. First, simulated annealing was used to minimize the objective function in Equation 24. Second, the method of Powell's in multi-dimensions began at the optimum values found by simulated annealing. Powell's method, then, ran using the same objective function to improve the draft produced by the algorithm of simulated annealing. The algorithm of simulated annealing began with a temperature of 100 and each cycle

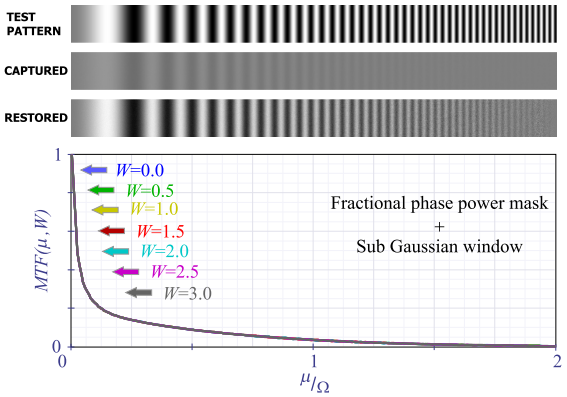

FIGURE 7. Fractional wavefront mask with a sub Gaussian window.

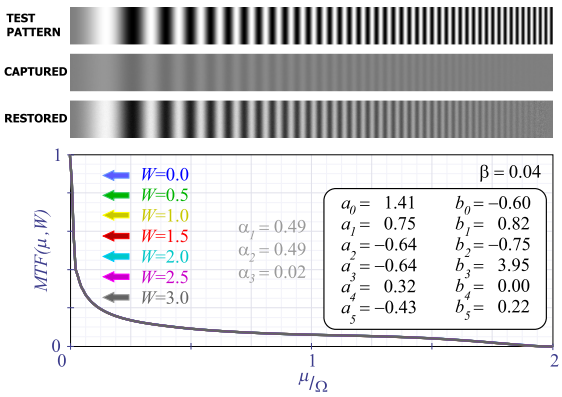

FIGURE 8. Resulting mask for $\beta = 0.04$.

TABLE 1. Experimental parameters and their values.

Simulated Annealing	
Initial temperature	100
Final temperature	10^{-6}
Number of temperatures	250
Number of iterations per temperature	100
Cooling schedule	Linear
Goal	10^{-6}
Cooling and heating cycles	10
Powell's Method	
Maximum number of iterations	200
Chebyshev polynomials	
Value of A in Equation 18	5
Value of B in Equation 18	5

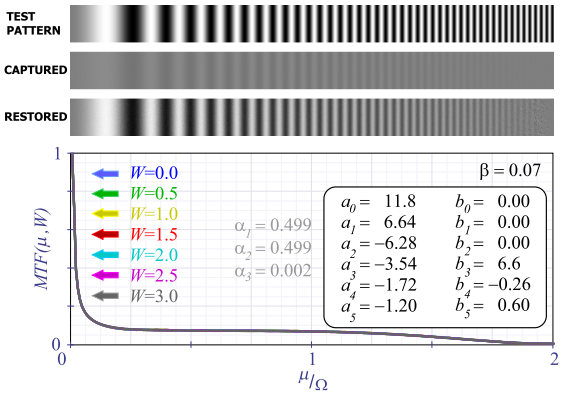

FIGURE 9. Resulting mask for $\beta = 0.07$.

ended with a final temperature of 1×10^{-6}. The number of temperatures was set to 250, and the number of iterations at each temperature was 100. The temperature followed a linear cooling schedule and 10 cycles of heating and cooling were performed. These were the values that offered the best results for this algorithm.

In order to adjust the number of iterations required by Powell's method in multi-dimensions, first, we executed the simulations using only 100 iterations. However, we noticed that by the time the algorithm had finished the iterations, the error was still decreasing. Consequently, we increased the number of iterations to 200 and added the option to stop early if no further improvements were possible. Because the draft produced by simulated annealing was frequently good, Powell's method stopped early without completing the 200 iterations. Thus, it was concluded that Powell's method did not require more than 200 iterations. The experimental parameters used in this study with their respective values are summarized in Table 1.

Figure 8 shows the MTF of the resulting mask when the algorithm proposed in this work ran with $\beta = 0.04$. The algorithm ran on a personal computer with Microsoft Windows 10 professional and an Intel Processor I7. The simulation ran for above 20 minutes on average. From Figure 8, it can be seen that MTF looks very similar for the seven values of W, in fact, it looks like one single graph and it is difficult to distinguish the seven graphs. However, some differences in the graphs can be observed in the electronic version of this paper when the figure size is increased by zooming in the document. The coefficients obtained by the optimization process of Equation 18 are also displayed in the figure. It can be observed that this mask has a very flat response even at very high frequencies. The captured image at the top reveals that this mask nicely preserves most of the image content. The restored image shows an excellent signal to noise ratio for most of the frequencies. However, there is some amount of noise that can be observed at very high frequencies.

Figure 9 shows another mask obtained by the method proposed in this work; in this case, β was set to 0.07. A quick inspection to graph reveals that the MTF exhibits very small changes for the seven values of W in the figure. In this case, the MTF reveals that it is impossible to attain a bigger amplitude in the full band. It seems that a bigger amplitude is attained at the cost of some amount of attenuation at very high frequencies. As expected, the restored image exhibits more noise than the one in Figure 8.

Figure 10 shows a mask obtained by the optimization process when $\beta = 0.11$. As can be seen from the figure when the amplitude of the MTF increases the bandwidth decreases. A quick inspection to the captured and restored images reveals the signal to noise ratio improves at low and medium frequencies, but it degrades at high frequency.

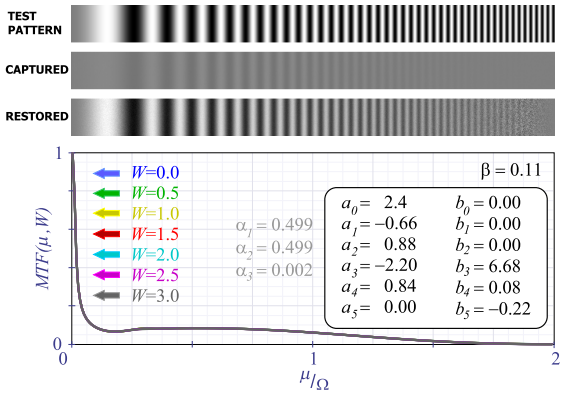

FIGURE 10. Resulting mask for $\beta = 0.11$.

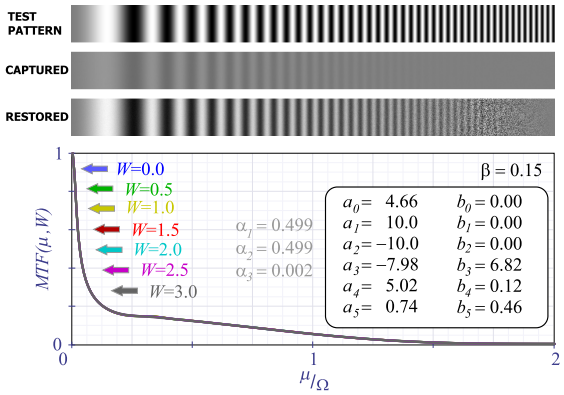

FIGURE 11. Resulting mask for $\beta = 0.15$.

Finally, Figure 11 displays a mask found by the Artificial Intelligence algorithm when $\beta = 0.15$. From the figure, it is clear that when the amplitude of the MTF increases, it is always at the sacrifice of the resolution of the image. That is, the signal to noise ratio at high and very high frequencies becomes poor.

Augmented reality involves a set of technologies that make use of an electronic device to view, directly or indirectly, a real-world physical environment that is combined with virtual elements [28]. One key factor in augmented reality is to match the depth of field of the virtual elements with the depth of field of the physical environment. This paper provides some insights that may be used in augmented reality to improve the performance of current systems.

Finally, we provide some directions for future work. First, we think that other methods such as Genetic Algorithms (GA) or Ant Colony Optimization (ACO) algorithms can also be considered to design the optical mask. Second, as the shape of the error function affects the performance of the optimization methods, we also think that it would be interesting to explore other error functions.

VIII. CONCLUSIONS

In this work, we present a method based on Artificial Intelligence to explore the existence of one or more optical masks with very low sensitivity to the focus error. We propose the use of Chebyshev polynomials to model the amplitude and the phase of the optical mask. This is the first time, to the best of our knowledge, that this type of mask is modeled using Chebyshev polynomials. Additionally, we propose three objective functions to optimize the properties of the mask: depth of field, resolution, and gathered light power. The Artificial Intelligence algorithm in combination with Powell's method in multi-dimensions uses a single objective function to design the mask with the desired properties. The paper includes the analysis of four masks found by the proposed algorithm. One classic mask in the field of optics was used to compare the results. Computer simulations showed that the obtained mask when $\beta = 0.04$ had the highest performance when compared with the other masks. The simulation results indicated that it is possible to adjust the parameters of the algorithm to target the desired mask properties.

ACKNOWLEDGMENT

The authors acknowledge the Faculty of Health Sciences of the University of Ottawa, and the DAIP, the University of Guanajuato for their sponsorship in the realization of this work. This work was developed during the sabbatical stay of Sergio Ledesma at the Faculty of Health Sciences in the University of Ottawa, Canada.

REFERENCES

[1] S. Pertuz, M. A. Garcia, and D. Puig, "Efficient focus sampling through depth-of-field calibration," *Int. J. Comput. Vis.*, vol. 112, no. 3, pp. 342–353, 2015.
[2] D. Guo, J. Yan, and X. Qu, "High quality multi-focus image fusion using self-similarity and depth information," *Opt. Commun.*, vol. 338, no. 1, pp. 138–144, Mar. 2015.
[3] D. Weigel, H. Babovsky, A. Kiessling, and R. Kowarschik, "Widefield microscopy with infinite depth of field and enhanced lateral resolution based on an image inverting interferometer," *Opt. Commun.*, vol. 342, no. 1, pp. 102–108, 2015.
[4] S. Ahn and J. Chong, "Segmenting a noisy low-depth-of-field image using adaptive second-order statistics," *IEEE Signal Process. Lett.*, vol. 22, no. 3, pp. 275–278, Sep. 2015.
[5] P. Kán and H. Kaufmann. "Physically-based depth of field in augmented reality," in *Proc. Eurographics*, 2012, pp. 89–92.
[6] G. Singh, S. R. Ellis, and J. E. Swan, II, "The effect of focal distance, age, and brightness on near-field augmented reality depth matching," *IEEE Trans. Vis. Comput. Graphics*, to be published.
[7] X. Liu and J. G. Rokne, "Depth of field synthesis from sparse views," *Comput. Graph.*, vol. 55, no. 1, pp. 21–32, 2016.
[8] D. C. Rompapas, A. Rovira, A. Plopski, C. Sandor, T. Taketomi, G. Yamamoto, H. Kato, and S. Ikeda, "EyeAR: Refocusable augmented reality content through eye measurements," *Multimodal Technol. Interact.*, vol. 22, no. 1, pp. 1–18, 2017.
[9] D. Chatzopoulos, C. Bermejo, Z. Huang, and P. Hui, "Mobile augmented reality survey: From where we are to where we go," *IEEE Access*, vol. 5, pp. 6917–6950, 2017.
[10] S. Ryu and C. Joo, "Design of binary phase filters for depth-of-focus extension via binarization of axisymmetric aberrations," *Opt. Express*, vol. 25, no. 24, pp. 30312–30326, 2017.
[11] M. Lopez-Ramirez, L. M. Ledesma-Carrillo, E. Cabal-Yepez, G. Botella, C. Rodriguez-Donate, and S. Ledesma, "FPGA-based methodology for depth-of-field extension in a single image," *Digit. Signal Process.*, vol. 70, no. 1, pp. 14–23, 2017.
[12] L. M. Ledesma-Carrillo, M. Lopez-Ramirez, C. A. Rivera-Romero, A. Garcia-Perez, G. Botella, and E. Cabal-Yepez, "Extended depth of field in images through complex amplitude pre-processing and optimized digital post-processing," *Comput. Elect. Eng.*, vol. 40, no. 1, pp. 29–40, 2014.

[13] T. E. Bishop and P. Favaro, "The light field camera: Extended depth of field, aliasing, and superresolution," *IEEE Trans. Pattern Anal. Mach. Intell.*, vol. 34, no. 5, pp. 972–986, May 2012.
[14] V. Boominathan, K. Mitra, and A. Veeraraghavan, "Improving resolution and depth-of-field of light field cameras using a hybrid imaging system," in *Proc. IEEE Int. Conf. Comput. Photogr. (ICCP)*, Santa Clara, CA, USA, May 2014, pp. 1–10.
[15] J. Ojeda-Castañeda, S. Ledesma, and C. M. Gomez-Sarabia, "Hyper Gaussian windows with fractional wavefronts," *Photon. Lett. Poland*, vol. 5, no. 1, pp. 23–25, 2013.
[16] K.-J. Hsu, K.-Y. Li, Y.-Y. Lin, A.-S. Chiang, and S.-W. Chu, "Optimizing depth-of-field extension in optical sectioning microscopy techniques using a fast focus-tunable lens," *Opt. Express*, vol. 25, no. 2, pp. 16783–16794, 2017.
[17] Y. Niu and F. Liu, "What makes a professional video? A computational aesthetics approach," *IEEE Trans. Circuits, Syst. Video Technol.*, vol. 22, no. 7, pp. 1037–1049, Jul. 2012.
[18] J. Ojeda-Castaneda, M. Rodriguez, and R. Naranjo, "Tunable phase masks for extended depth of field," in *Proc. Prog. Electromagn. Res.*, 2010, pp. 531–533.
[19] V. N. Boddeti and B. V. K. V. Kumar, "Extended-depth-of-field iris recognition using unrestored wavefront-coded imagery," *IEEE Trans. Syst., Man, Cybern. A, Syst. Humans*, vol. 40, no. 3, pp. 495–508, May 2010.
[20] C. Ferran, S. Bosch, and A. Carnicer, "Design of optical systems with extended depth of field: An educational approach to wavefront coding techniques," *IEEE Trans. Educ.*, vol. 55, no. 2, pp. 271–278, Oct. 2012.
[21] E. R. Dowski and W. T. Cathey, "Extended depth of field through wavefront coding," *Appl. Opt.*, vol. 34, no. 11, pp. 1859–1866, 1995.
[22] J. Ojeda-Castaneda, E. Yépez-Vidal, and E. Garcia-Almanza, "Complex amplitude filters for extended depth of field," *Photon. Lett. Poland*, vol. 2, no. 4, pp. 162–164, 2010.
[23] W. H. Press, S. A. Teukolsky, W. T. Vetterling, and B. P. Flannery, *Numerical Recipes in C++: The Art of Scientific Computing*, 3rd ed. Cambridge, U.K.: Cambridge Univ. Press, 2007, pp. 549–555.
[24] S. J. Russel and P. Norvig, *Artificial Intelligence: A Modern Approach*. London, U.K.: Pearson, 2014, pp. 122–204.
[25] S. Ledesma, M. Torres, D. Hernandez, G. Avina, and G. Garcia, "Temperature cycling on simulated annealing for neural network learning," in *Proc. MICAI*. Berlin, Germany: Springer-Verlag, 2007, pp. 161–171.
[26] S. Ledesma, G. Avina, and R. Sanchez, "Practical considerations for simulated annealing implementation," in *Simulated Annealing*. London, U.K.: InTech, 2008, pp. 401–420.
[27] R. Ben-Ari, "A unified approach for registration and depth in depth from defocus," *IEEE Trans. Pattern Anal. Mach. Intell.*, vol. 36, no. 6, pp. 1041–1055, Jun. 2014.
[28] P. Fraga-Lamas, T. M. Fernández-Caramés, O. Blanco-Novoa, and M. A. Vilar-Montesinos. "A review on industrial augmented reality systems for the industry 4.0 shipyard," *IEEE Access*, vol. 6, pp. 13358–13375, 2018.

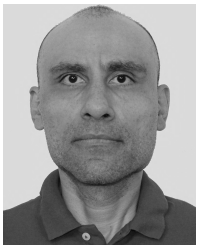

SERGIO LEDESMA received the M.S. degree from the University of Guanajuato, in 1992, while working on the setup of Internet in Mexico, and the Ph.D. degree from the Stevens Institute of Technology, Hoboken, New Jersey, in 2001. After graduating, he worked for Barclays Bank as part of the IT-HR group. He has worked as a Software Engineer for several years, and he is the creator of the software Neural Lab, Wintempla and TexLab. He is a Research Professor with the University of Guanajuato, Mexico. Currently, he is on a sabbatical stay at the University of Ottawa, Canada. His research interests include artificial intelligence and software engineering.

MARIO-ALBERTO IBARRA-MANZANO received the B.Eng. degree in communication and electronic engineering and the M.Eng. degree in electric engineering from the University of Guanajuato, Salamanca, Mexico, in 2003 and 2006, respectively, and the Ph.D. degree (Hons.) from the Institut National des Sciences Appliquées, Toulouse, France, in 2011. He is currently an Assistant Professor with the Electronics Engineering Department, Universidad de Guanajuato. His research interests include digital design on FPGA for image processing applied on autonomous robots and real-time systems.

EDUARDO CABAL-YEPEZ received the M.Eng. degree from Facultad de Ingenieria Mecanica Electrica y Electronica (FIMEE), Universidad de Guanajuato, Mexico, in 2001, and the Ph.D. degree from the University of Sussex, U.K., in 2007. In 2008, he joined the Division de Ingenierias, Campus Irapuato-Salamanca, Universidad de Guanajuato, where he is a leading Professor and Dean of the Multidisciplinary Studies Department. He has been author/coauthor of more than 31 research papers published in journals registered in the Journal Citation Report (JCR). His current research interests include digital instrumentation, digital image and signal processing, artificial intelligence, robotics, smart sensors, real-time processing, mechatronics, FPGAs, power quality, embedded systems, etc. He serves as an Area Editor for *Computers and Electrical Engineering* (Elsevier) and an Associate Editor for *Digital Signal Processing* (Elsevier) and for the IEEE TRANSACTIONS ON INSTRUMENTATION AND MEASUREMENT. He is an active member of the IEEE Instrumentation and Measurement Society, the IEEE Industrial Electronics Society, and the IEEE Signal Processing Society.

DORA-LUZ ALMANZA-OJEDA received the B.S. degree in electronics engineering and the M.S. degree in electrical engineering from the University of Guanajuato, Salamanca, Mexico, in 2003 and 2005, respectively, and the Ph.D. degree from the University of Toulouse III: Paul Sabatier, Toulouse, France, in 2011. She is currently an Assistant Professor with the Electronics Engineering Department, University of Guanajuato. Her research interests include embedded vision for controlling autonomous robots and real-time systems.

PASCAL FALLAVOLLITA received the Postdoctoral Fellowship in collaboration with the teams at Queen's University (The Perk Lab) and the Johns Hopkins School of Medicine (JHU) from 2008 to 2010. Afterward, he led the research activities at one of the two labs of the Chair for Computer-Aided Medical Procedures, Technische Universität München, considered to be among the world-class leaders in translational research and medical augmented reality. His research has produced many publications and patents, with several successful translational research studies. His main research is to promote healthy aging. His research interests include augmented reality/virtual reality for medical education and rehabilitation, surgical simulation and training, intraoperative imaging and surgical navigation, development of surgical systems, and user interfaces for therapy delivery.